R & M No. 3849

R & M No. 3849

PROCUREMENT EXECUTIVE, MINISTRY OF DEFENCE

Aeronautical Research Council
Reports and Memoranda

MEASUREMENTS OF PRESSURE DISTRIBUTIONS AND PRESSURE DRAGS AT ZERO INCIDENCE ON BOTH BLUNT AND SHARP AXISYMMETRIC FOREBODIES AT A MACH NUMBER OF 3

by

L.C. Ward
Aerodynamics Department, R.A.E., Bedford

London: Her Majesty's Stationery Office
£8 NET

UDC 533.696.7 : 533.696.42 : 533.6.048.2 : 533.6.013.122 : 533.6.011.5

MEASUREMENTS OF PRESSURE DISTRIBUTIONS AND PRESSURE DRAGS AT ZERO INCIDENCE ON BOTH BLUNT AND SHARP AXISYMMETRIC FOREBODIES AT A MACH NUMBER OF 3

By L. C. Ward

Aerodynamics Department, RAE Bedford

REPORTS AND MEMORANDA No.3849*

November 1976

SUMMARY

A collection of surface pressure distributions measured on a number of axisymmetric forebodies at zero incidence and a Mach number of 3 is presented. Integrated pressure drags are compared with the theoretical drags of sharp cones having the same forebody fineness ratios, showing that significant drag reductions can be achieved at this Mach number by the suitable use of nose blunting, leading also to an increase of usable volume in the forebody. Comparisons are also made with published data for determining the pressure drag of spherically blunted cones.

* Replaces RAE Technical Report 76160 - ARC 37355

CONTENTS

1 INTRODUCTION

It has been shown, both experimentally[1] and theoretically[2], that at supersonic and hypersonic speeds a suitable amount of spherical nose blunting on a cone can give an overall forebody pressure drag less than that of a sharp cone with the same forebody fineness ratio. As part of a series of wind-tunnel tests aimed at quantifying the effects of various types of nose blunting on different forebody profiles, pressure distributions were measured over the surfaces of sixteen forebodies at a freestream Mach number of 3. The forebody shapes investigated were spherically-blunted single and double cones, spherically-blunted tangent ogives, truncated cones, and three-quarter power-law profiles. A description of these tests, and a collection of the results obtained at zero incidence are presented in this Report. Comparisons are shown between the experimental pressure drags, the theoretical drag of sharp cones, and data taken from the Engineering Sciences Data Unit item number 68021 [1] on spherically-blunted cones without afterbodies.

2 WIND TUNNEL, MODELS AND INSTRUMENTATION

The models were tested in the RAE (Teddington) 15in × 10in blowdown wind tunnel, the freestream Mach number at the model location being 3.00. The stagnation pressure was kept constant at $552 \times 10^3 N/m^2$, giving a freestream Reynolds number per mm of 4.18×10^4 for all the models. No boundary layer transition fixing devices were used on any of the models.

The models were attached to the sting by means of an adaptor containing 'O' ring seals on each of the seven pressure tubes. The general arrangement of a model, adaptor and sting as mounted in the wind tunnel is shown in Fig.1, together with a cross-section through one model tube, the adaptor and part of the sting. By slackening the adaptor fixing screw, both the adaptor and the model could be rotated through 51.43 degrees (one seventh of a circle), without disconnecting any of the plastic tubing.

The sting could accommodate only seven pressure tubes, so in order to obtain an adequate pressure distribution two separate models, each with different hole locations, were manufactured for each body profile. The non-dimensional parameters of the bodies are given in Table 1, the notation for which is defined in Fig.2 for the different types of body shape tested. As there are two definitions of the bluntness ratio in frequent use (i.e. 2r/D or d/D), both ratios are given. Drawings showing the actual model dimensions in mm are given later with each set of results.

The pressure measuring holes of diameter 0.5mm were arranged in a spiral pattern around each model, thereby helping to eliminate downstream interference effects between adjacent holes. All the tappings were carefully inspected prior to the tunnel tests to ensure that there were no burrs either inside the holes, or on the body surface around the holes.

The surface pressures were measured using a strain-gauge transducer mounted in a 48 way pressure-scanning switch situated outside the wind tunnel. The switch was of the stepping variety, pressure settling dwell times on the ports prior to data recording being determined from a number of initial wind-tunnel runs. Each port of the scanning switch was 'O' ring sealed, with the transducer being subjected to a vacuum in between ports, thus eliminating transducer hysteresis effects that would arise from the different pressure levels being measured. Known reference pressures were applied to the initial three ports of the switch, thereby allowing a check on the transducer calibration to be made for each scan of the model pressures. The wind-tunnel stagnation pressure was recorded using a transducer with a higher pressure range mounted in a module complete with its own pressure calibration system. The calibration pressures were measured with either a Texas gauge for the high values, or a vacuum gauge for the very low pressures.

The data recording equipment consisted of a data-logger manufactured by Digital Measurements Ltd. which scanned the transducer outputs at low level. After amplification, the resulting high level analogue signals were converted to digital form and finally recorded on paper tape. The wind-tunnel stagnation pressure was recorded for each pressure switch reading, thereby allowing the surface pressures to be corrected for variations in the freestream pressure.

The transducer excitation voltages and the amplifier gain were set so that the overall pressure range of each transducer produced changes in the amplified outputs of the order of 10000 counts. The observed repeatability in the outputs obtained from the known reference pressures was approximately ±2 counts. Applying this change to both transducers, a maximum variation in p/p_0 and C_p of ±0.006 and ±0.0012, respectively, would be expected over the complete range of the pressure switch transducer.

3 PRESENTATION OF THE RESULTS

The pressure distribution at zero incidence for each forebody is presented in terms of p/p_0 and C_p (Y/D) in Figs.3 to 18; each figure also gives details of the

forebody profile. The origin for the XY coordinate system was chosen to be at the model base, with the exceptions of models 16 to 23 where the origin was located at the junction between the forebody and the short cylindrical afterbody, since no pressures were measured on the afterbody section.

The results shown are the average pressure values obtained from seven tunnel runs, each at different model roll angles, to minimise errors due to asymmetries in the tunnel flow or model attitude.

For some of the blunted profiles, notably models 16 to 19 (Figs.9 and 10) and models 24 to 27 (Figs.13 and 14), the blunted area was too small to include enough pressure tappings for an adequate definition of the pressure distributions to be obtained. In the case of bodies with spherical blunting, recourse was made to previously published data[3] showing the pressure distribution around a hemisphere. The extracted data were then scaled to allow for the different nose radii, the test results being used to plot the intermediate values of C_p Y/D shown in the figures. The same process was used for the truncated bodies, this time using data for a disc[4] as given in Fig.19. This figure also presents data for two blunt high-angled cones[4].

The pressure distributions were integrated to obtain the forebody pressure drag (C_{D_p}), values of which are given in Table 1 together with values (where possible) determined from ESDU Item 68021 [1]. For the spherically-blunted cones, there is good agreement between the experimental values of C_{D_p} and the ESDU data for two out of the four profiles (models 12 and 13, 20 and 21). In the case of the 7.5 degree cone with d/D = 0.2 (models 16 and 17) the difference between the two values of C_{D_p} is probably due to the spacial inadequacy of the measured pressure distribution, as mentioned above, giving an erroneous value to the forebody pressure drag. This may also explain the difference observed with models 8 and 9. Agreement between the two values is not, however, very good for the two blunted tangent ogives (models 32 and 33, 34 and 35) probably because the ESDU data is based on results for blunted cones.

As there are no consistent geometrical constants or variables throughout the range of bodies tested, the pressure drags have been compared with the theoretical pressure drag coefficients of sharp cones[5] for fineness ratios between 0 and 3.2 (Figs.20 and 21). For sharp cones with fineness ratios less than 0.43 (i.e. when the bow shock-wave is detached) the drag coefficients are

assumed to lie on the dotted line drawn from the theoretical drag coefficient of a fineness ratio 0.43 sharp cone, and through the experimental values obtained for the sharp cone and the disc with fineness ratios of 0.182 and 0 respectively. Figs.20 and 21 also give the minimum drag obtainable from spherical blunting as a function of the fineness ratio as determined from the ESDU data item[1], showing how the optimum bluntness ratio decreases with increasing fineness ratio.

From Fig.20, it can be seen that at values of fineness ratio less than that for shock detachment on a sharp cone ($f \leq 0.43$), all but one of the bodies tested had a lower pressure drag than a sharp cone of the same fineness ratio, substantial reductions in drag stemming from quite large amounts of blunting and truncating. This is borne out by the ESDU data which suggests that at these low fineness ratios the bodies with the lowest drags would be circular arc profiles with bluntness ratios between a hemisphere ($d/D = 1.0$) and a disc (i.e. a blunt cone with a bluntness ratio of infinity).

At the higher fineness ratios between 2.0 and 3.2, all the blunted and truncated single cones that were tested gave pressure drags higher than sharp cones of the same fineness ratio, with the exception of models 16 and 17, though in this case the experimental data is suspect (see above). This finding is not surprising as the minimum bluntness ratio tested was 0.2, and the ESDU data shows that for minimum drag the bluntness ratio would have to be less than 0.2. Both of the blunted tangent ogives likewise give higher drags than for the equivalent sharp cone of fineness ratio 2, though it should be noted that the difference is small for the tangent ogive of bluntness ratio 0.3. Thus it would appear that a significant amount of blunting on a tangent ogive is possible without much of a drag penalty relative to a sharp cone of the same fineness ratio.

It is interesting to note that the blunted double cones (models 24 and 25, 26 and 27) have almost identical pressure drags to the three-quarter power law bodies of the same fineness ratio (models 28 and 29, 30 and 31) which are generally accepted as being among the better low-drag nose shapes.

4 CONCLUSIONS

Surface pressure distributions have been presented for a range of different axisymmetric forebody profiles at zero incidence and at a Mach number of 3. The integrated pressure drags have been compared with the theoretical pressure drags of sharp cones and with data extracted from ESDU data Item 68021 on blunted cones.

The main conclusions from this work are:-

(a) for forebody fineness ratios less than 0.6, the pressure drag of a spherically-blunted or truncated cone is substantially lower than that of a sharp cone of the same fineness ratio;

(b) as the forebody fineness ratio increases, the amount of blunting required for minimum pressure drag decreases;

(c) only a small amount ($d/D \simeq 0.2$) of spherical blunting or truncation can be used on cones or tangent ogives with fineness ratios between 2 and 3.2 if pressure drags comparable with those of sharp cones with the same fineness ratio are to be obtained;

(d) the published data[1] on the pressure drag of spherically blunted cones without afterbodies show the same trends as the test results for blunted cones with afterbodies, though the absolute levels are not always the same;

(e) the published data[1] disagree with the pressure drags measured on blunted tangent ogives;

(f) appropriately-proportioned blunted double-cones can have the same pressure drags as three-quarter power law bodies of the same fineness ratio.

The intelligent use of some form of nose blunting has a number of advantages over a sharp nose, not only in reduced pressure drag. These advantages include a higher internal volume, and a lower peak heat transfer rate to the body nose. Thus theoretical methods are required at any relevant Mach number for determining the optimum type and amount of bluntness for practical body shapes of given fineness ratio. This collection of pressure measurements should provide a good basis for checking methods developed for use at supersonic Mach numbers.

Table 1

SUMMARY OF RELEVANT BODY GEOMETRIES, INTEGRATED PRESSURE DRAGS AND FOREBODY DRAGS FROM REF.1

Model No.	f	2r/D	d/D	θ_1°	θ_2°	R/D	C_{D_p}		Forebody shape
							Expt.	Ref.1	
6 and 7	0.163	0.133	0.390	70			1.4760		Spherically blunted cone
8 and 9	0.441	0.198	0.280	45			1.1520	1.100	" " "
12 and 13	0.382	0.396	0.560	45			1.0920	1.112	" " "
16 and 17	3.125	0.198	0.200	7.5			0.0600	0.090	" " "
20 and 21	2.466	0.397	0.400	7.5			0.1600	0.162	" " "
36	0.174	0.086	0.250	70			1.4500		" " " (Ref.4)
37	0.086	0.043	0.250	80			1.5320		" " " (Ref.4)
4 and 5	0.182	0	0	70			1.4880		Sharp cone
10 and 11	0.400		0.200	45			1.0520		Truncated cone
14 and 15	0.300		0.400	45			1.0740		" "
18 and 19	3.038		0.200	7.5			0.0940		" "
22 and 23	2.279		0.400	7.5			0.2780		" "
38	0		1	90			1.5660		Disc (Ref.4)
24 and 25	3	0.098	0.100	10.35	6.94		0.0614		Spherically blunted double cone
26 and 27	2	0.121	0.125	14.36	11.01		0.1232		" " " "
28 and 29	3						0.0612		$\frac{3}{4}$ power law
30 and 31	2						0.1226		" "
32 and 33	2	0.279	0.300			5.214	0.1625	0.187	Spherically blunted tangent ogive
34 and 35	2	0.584	0.600			7.625	0.2920	0.355	" " " "

SYMBOLS

C_{D_p}	forebody pressure drag coefficient $8\int_0^{0.5} C_p(Y/D)\,d(Y/D)$
C_p	pressure coefficient $(p - p_\infty)/q$
$C_{p\ vac}$	pressure coefficient when $p = 0$ i.e. vacuum conditions
D	maximum body diameter
d	diameter of nose blunting (see Fig.2)
f	forebody fineness ratio L/D
L	overall forebody length
p	surface pressure
p_0	freestream stagnation pressure
p_∞	freestream static pressure
q	kinetic pressure
R	radius of tangent ogive profile (see Fig.2)
r	radius of body at junction between spherical nose blunting and forebody profile (see Fig.2)
X	axial distance along body centre line (positive upstream)
Y	radial distance from X axis
θ_1 and θ_2	angles between conical sections and the X axis (see Fig.2)

REFERENCES

No.	Author	Title, etc.
1	-	Foredrag of spherically blunted cones in supersonic flow. Engineering Sciences Data Unit Item 68021 (1968)
2	P.G. Pugh L.C. Ward	A parametric study of the use of nose blunting to reduce the supersonic wave drag of forebodies. ARC Current Paper 1271 (1974)
3	P.G. Pugh J.W. Peto L.C. Ward	Experimental verification of predicted static hole size effects on a model with large streamwise pressure gradients. NPL Aero Report 1313 (ARC 31900) (1970)
4	J.F. Campbell D.H. Tudor	Pressure distributions on 140°, 160° and 180° cones at Mach numbers from 2.30 to 4.63 and angles of attack from 0° to 20°. NASA TN D-5204 (1969)
5	Ames Research Staff	Equations, tables, and charts for compressible flow. NACA Report 1135 (1953)

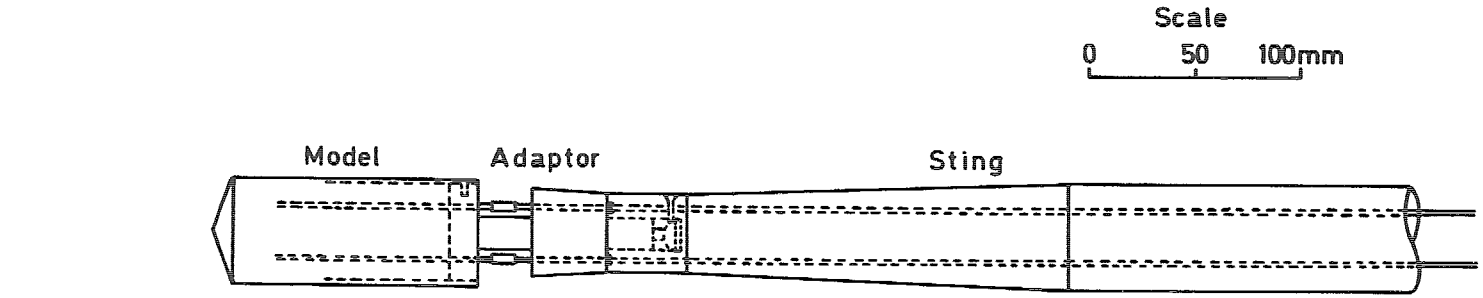

General arrangement

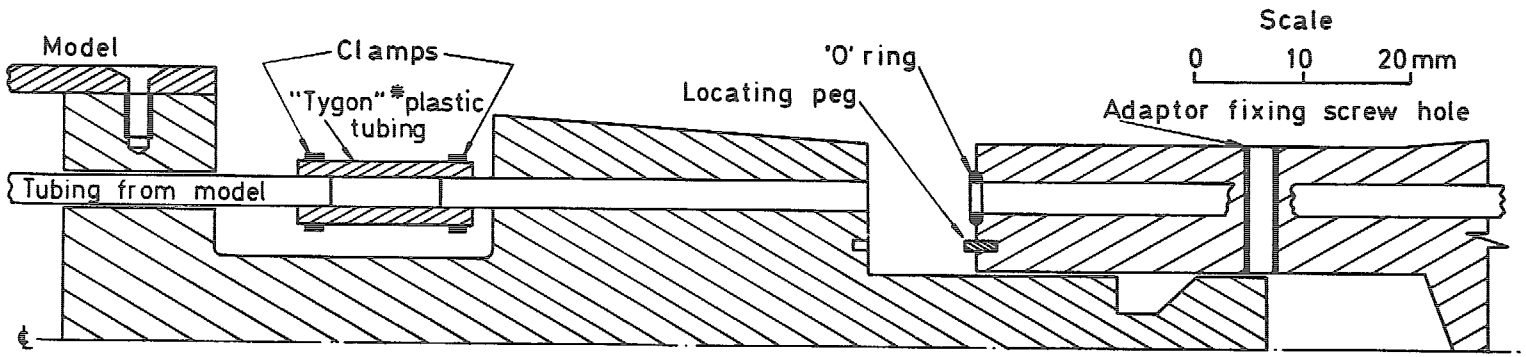

Adaptor and 'O'ring sealing details

* Proprietary trade name - formulation R3603

Fig 1 General arrangement of model mounting on the wind-tunnel sting, and details of 'O' ring adaptor

Fig 2

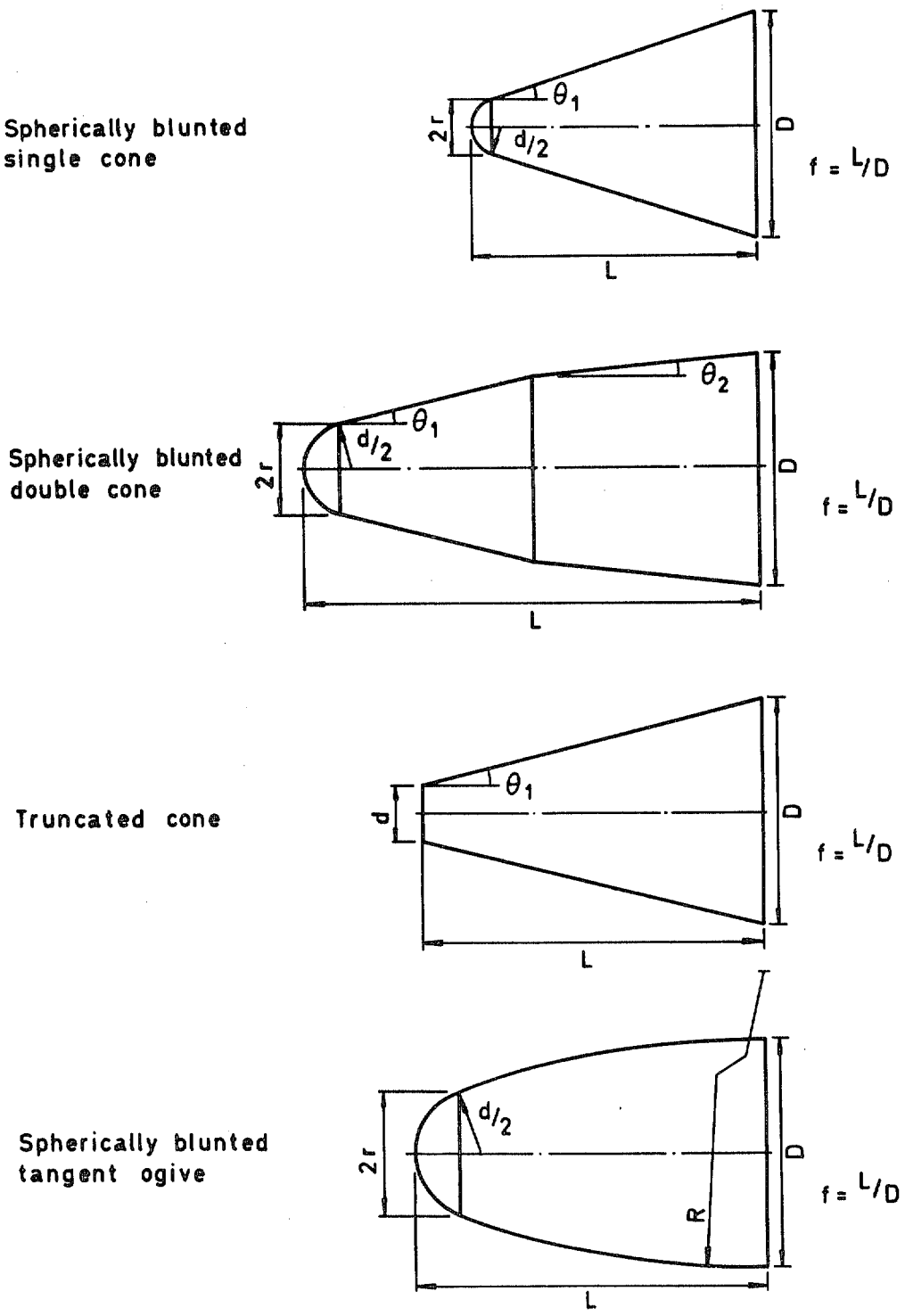

Fig 2 Geometrical nomenclature used for the forebodies. Cylindrical afterbodies are not shown

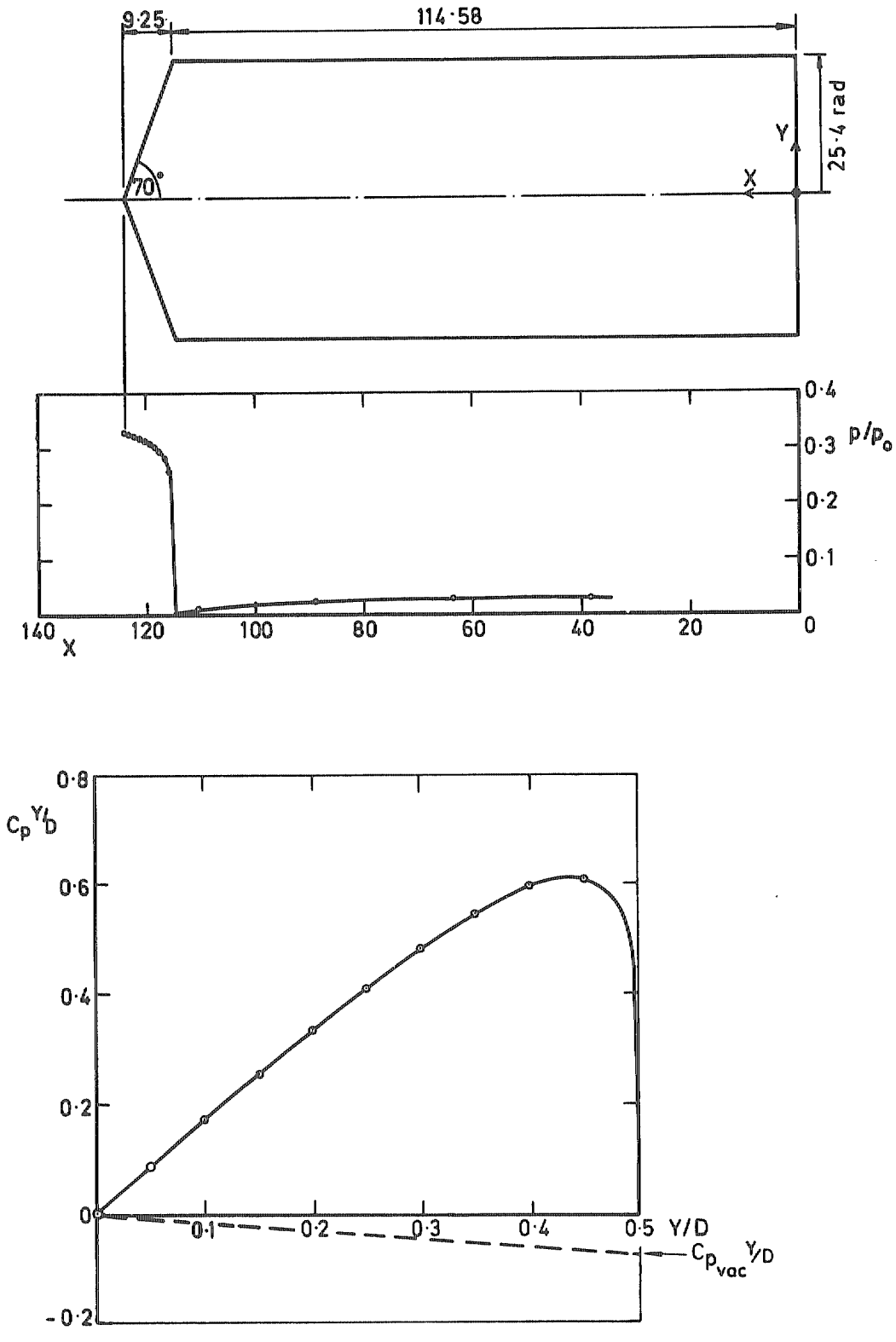

Fig 3 Experimental results. Models 4 and 5

Fig 4

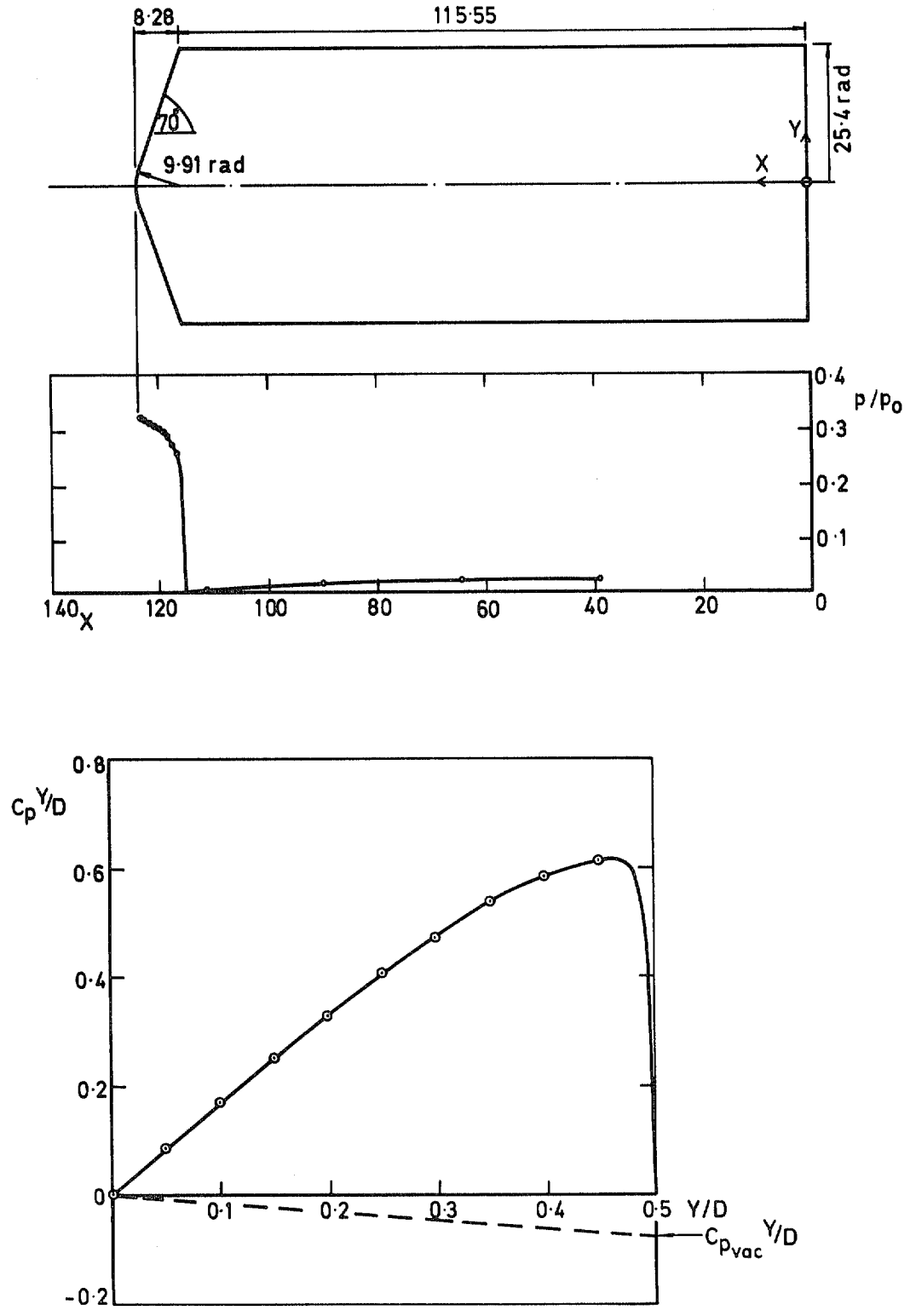

Fig 4 Experimental results. Models 6 and 7

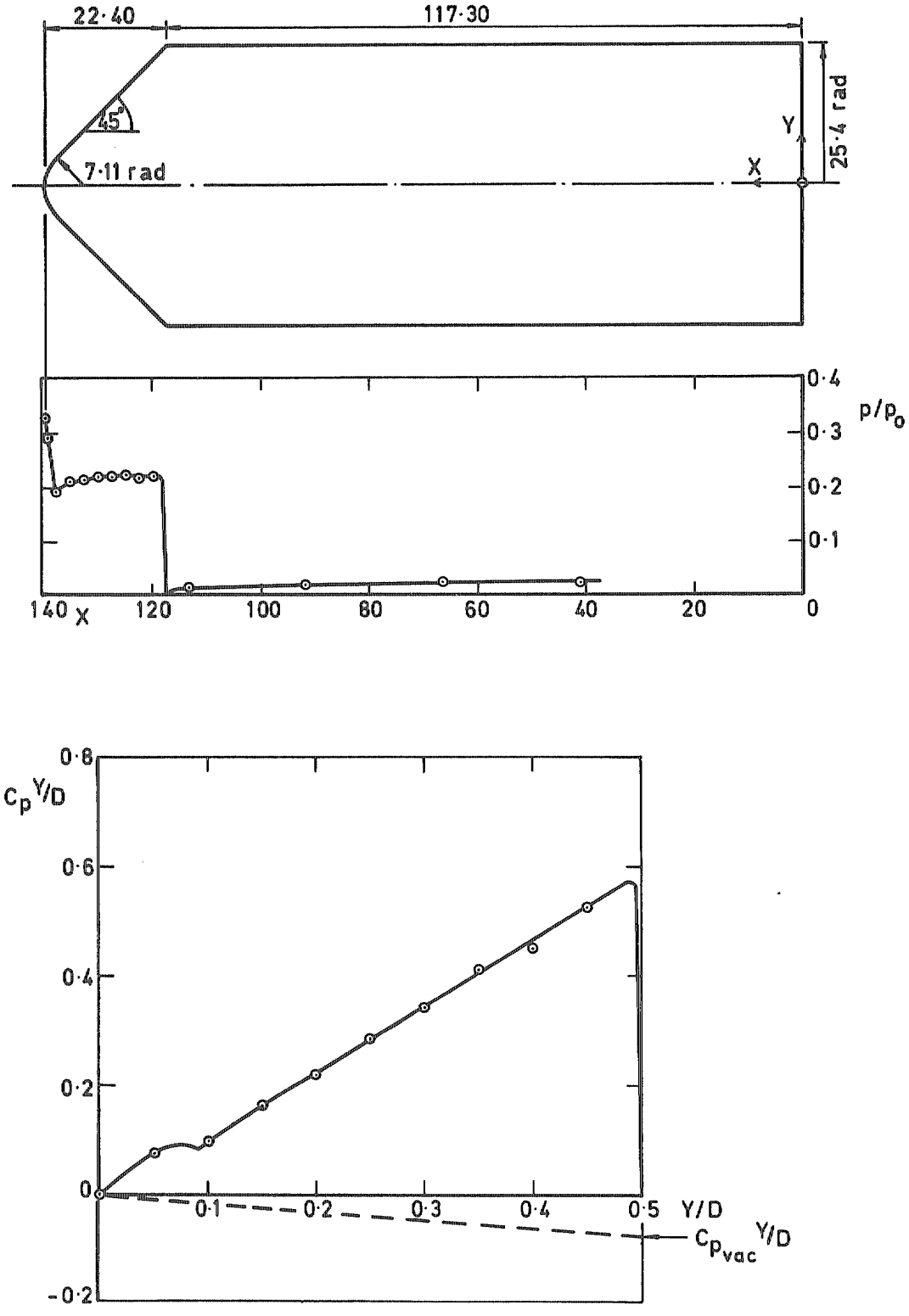

Fig 5 Experimental results. Models 8 and 9

Fig 6

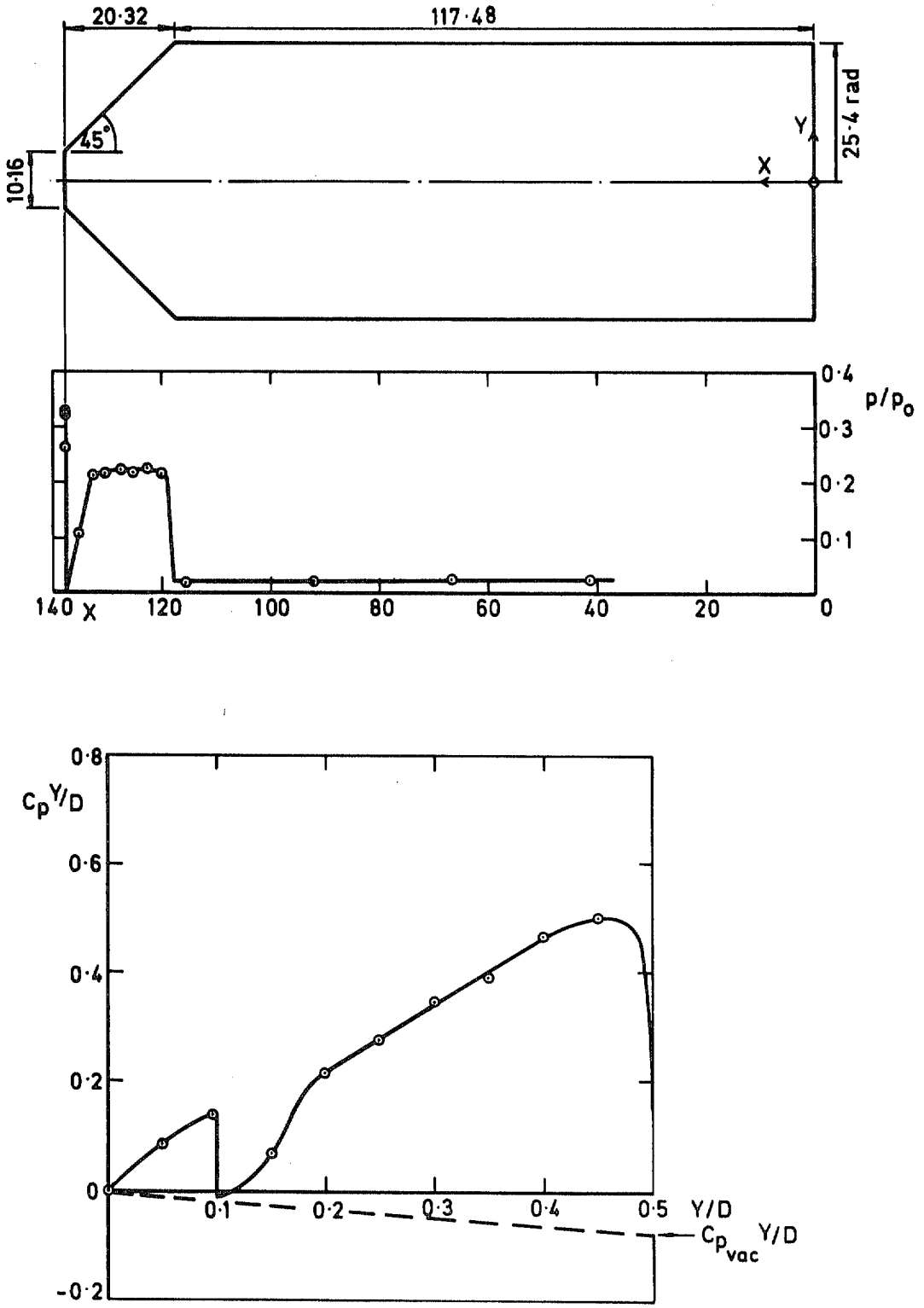

Fig 6 Experimental results. Models 10 and 11

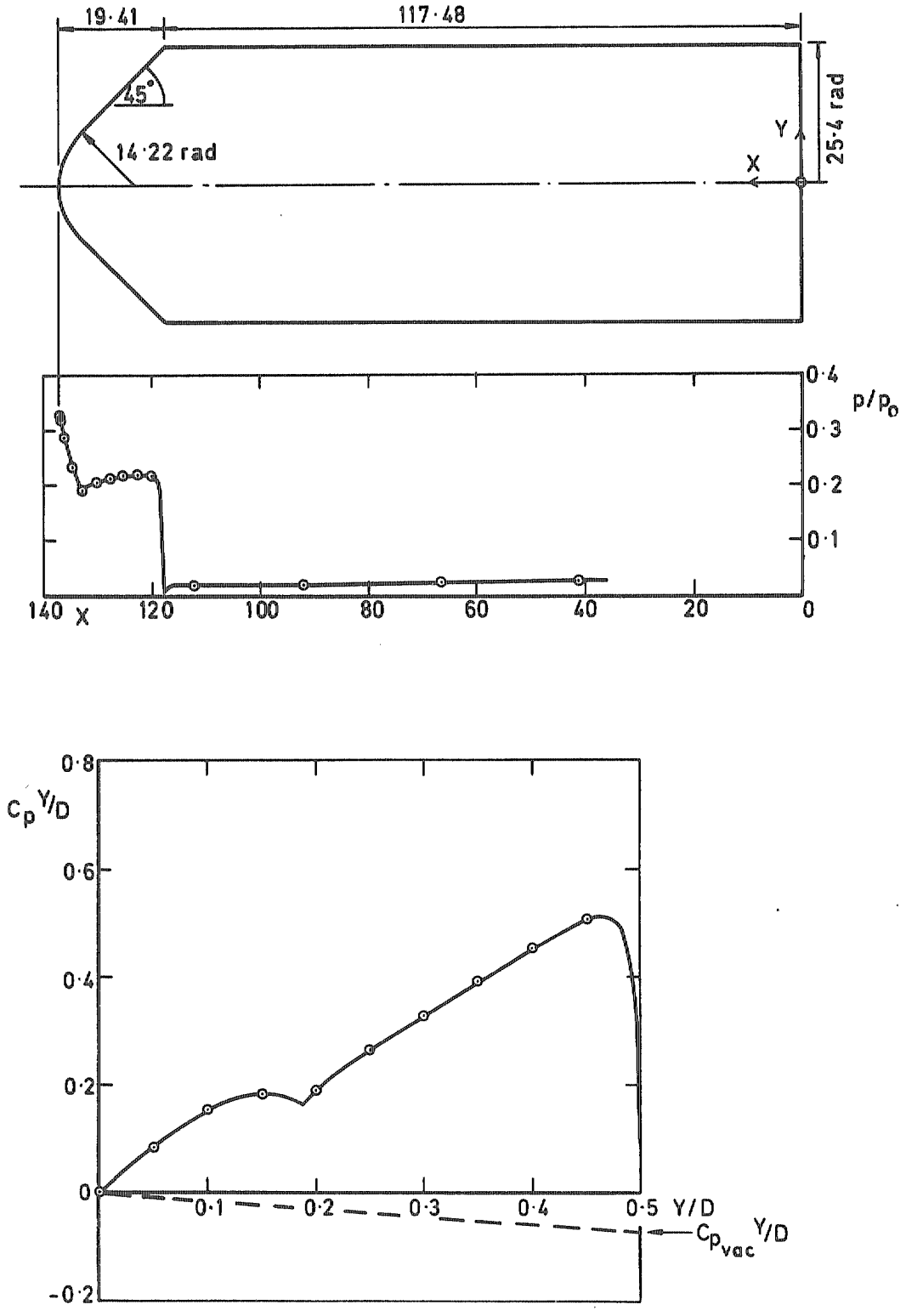

Fig 7 Experimental results. Models 12 and 13

Fig 8

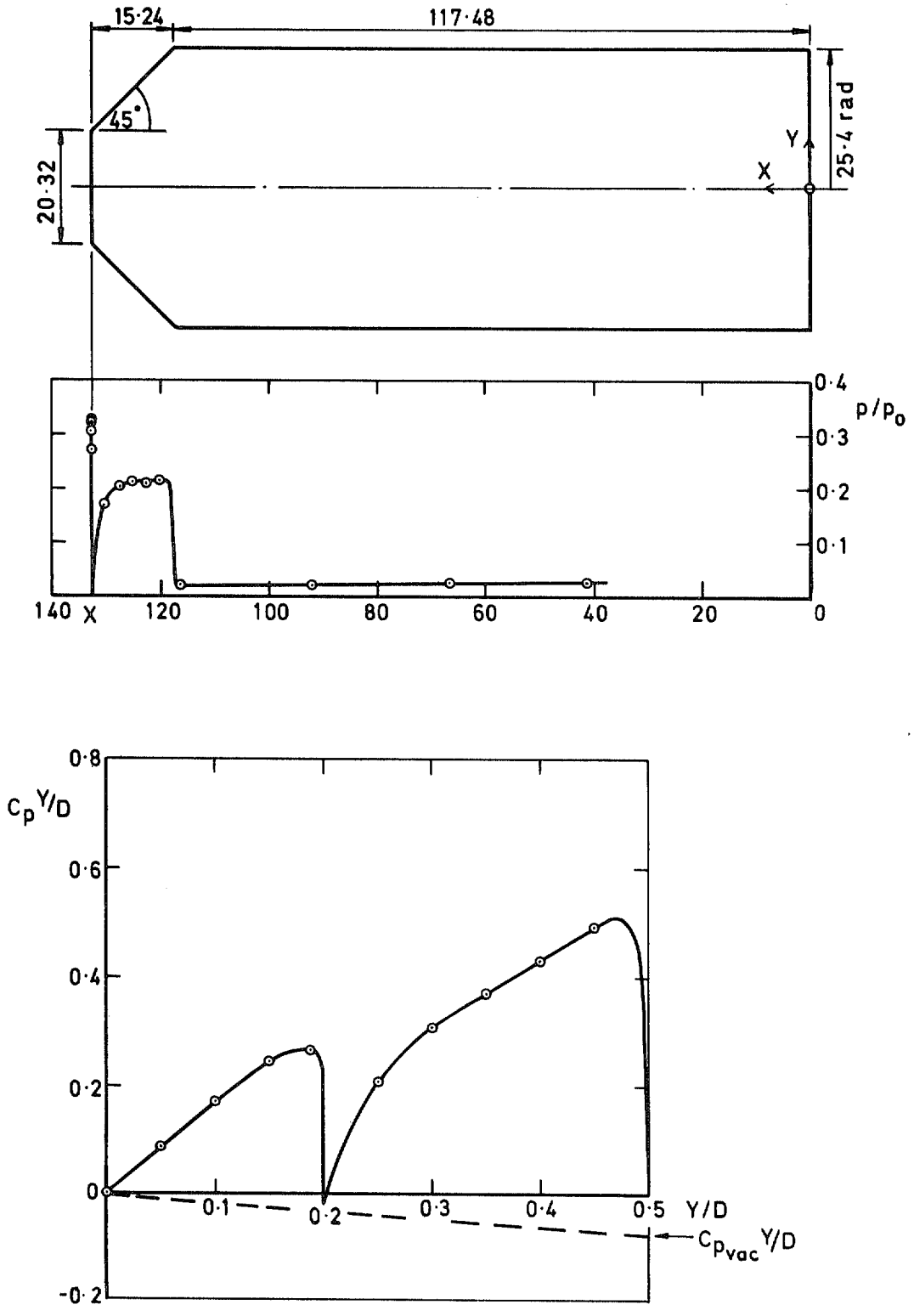

Fig 8 Experimental results. Models 14 and 15

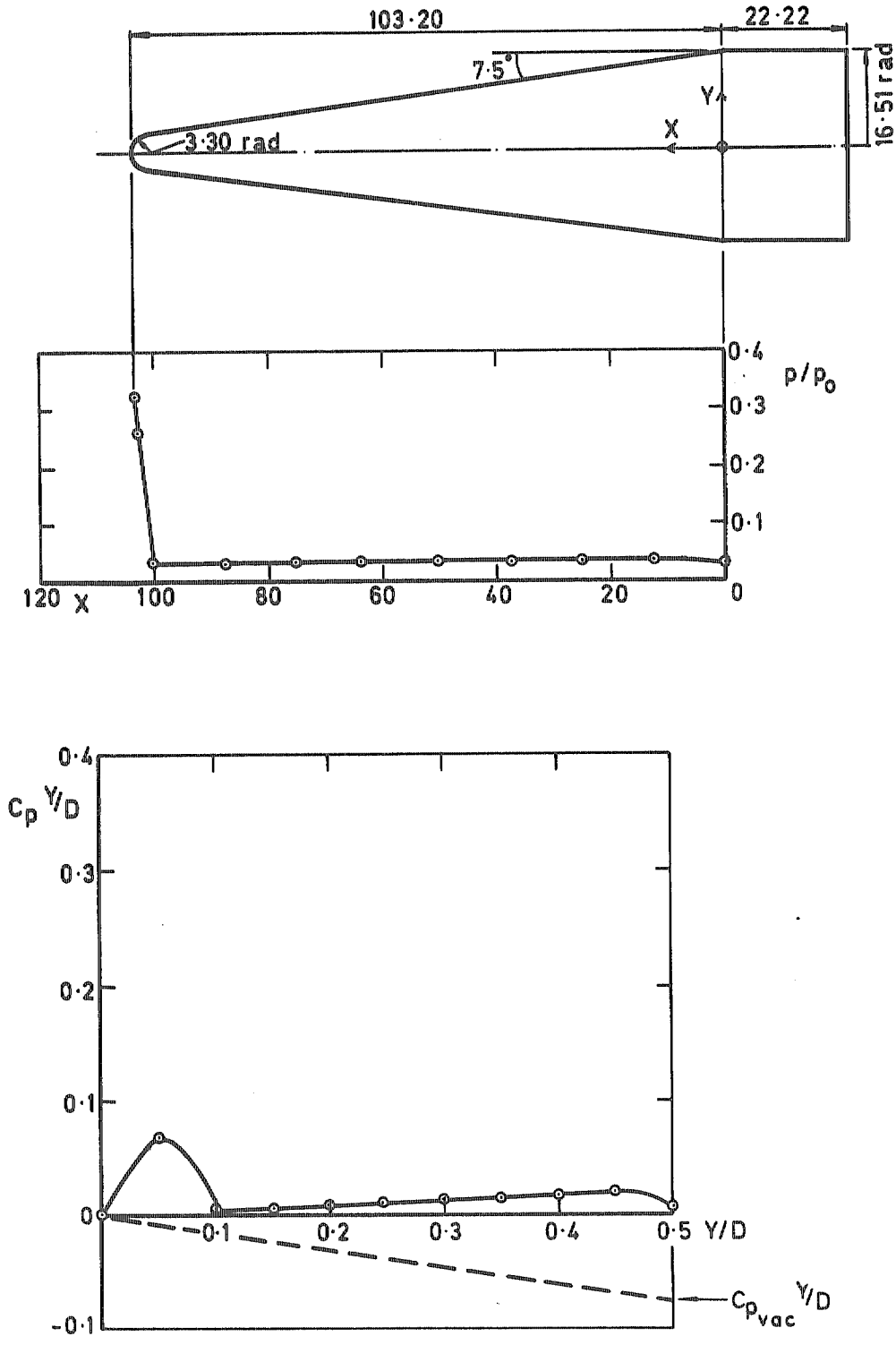

Fig 9 Experimental results. Models 16 and 17

Fig 10

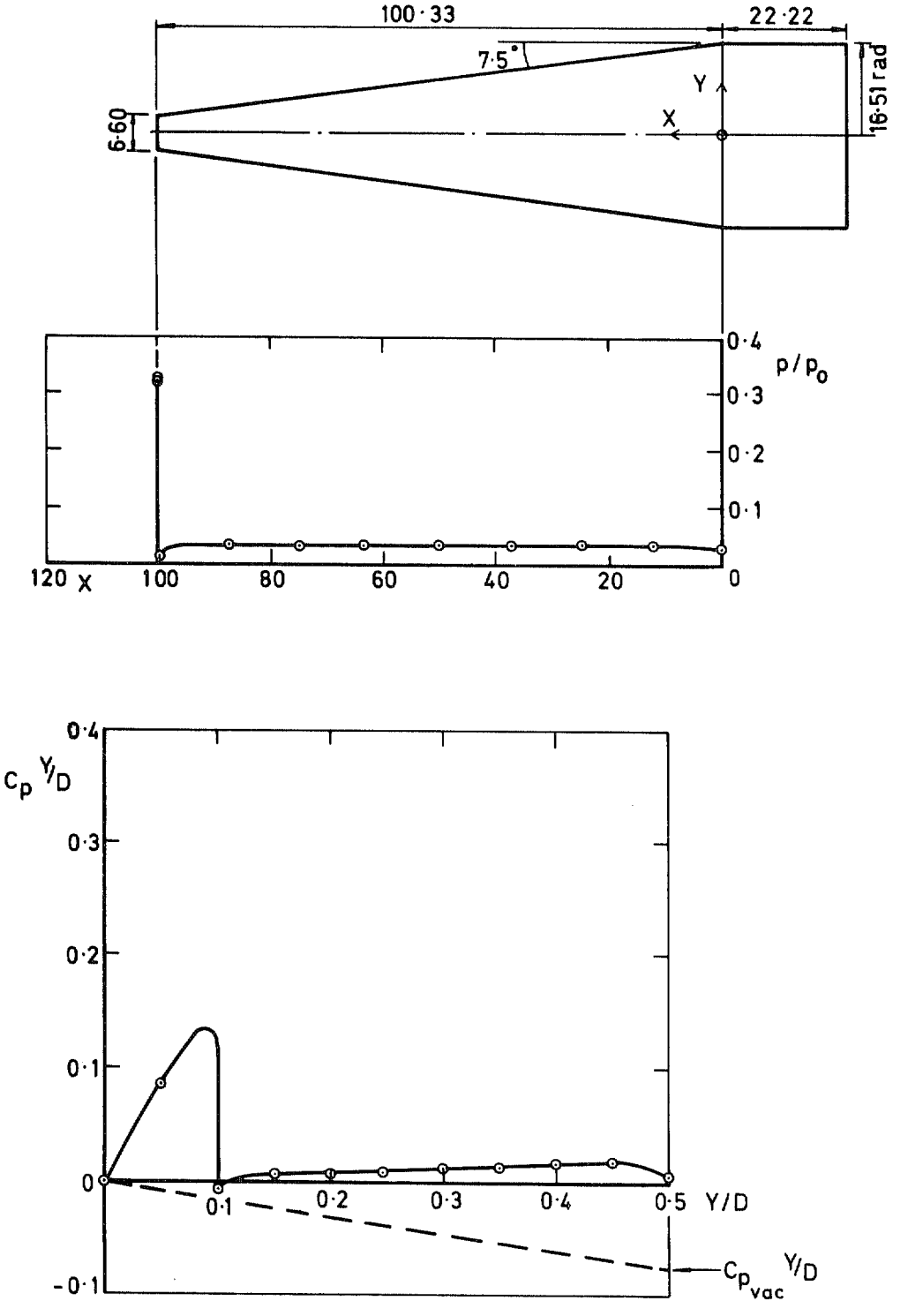

Fig 10 Experimental results. Models 18 and 19

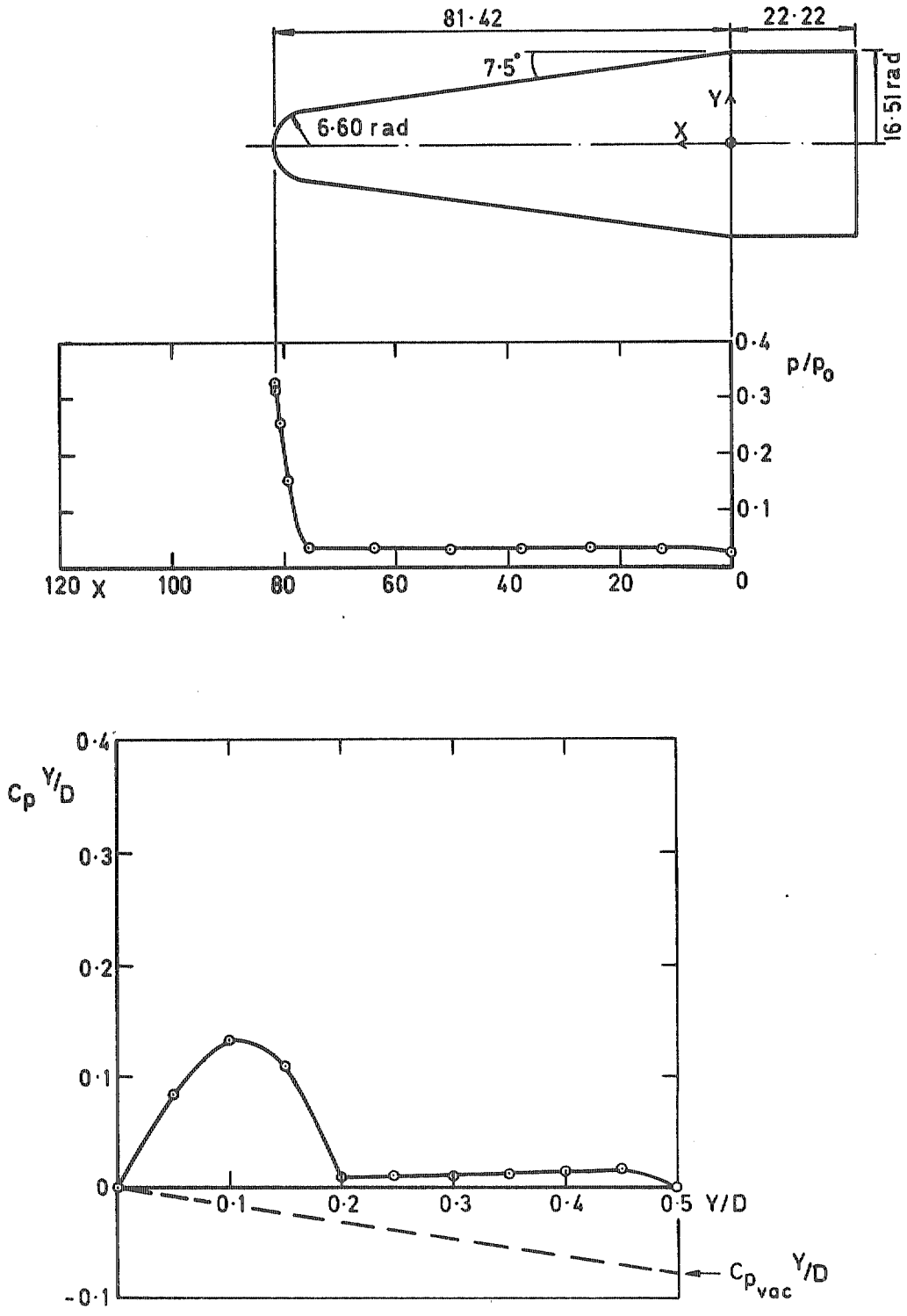

Fig 11 Experimental results. Models 20 and 21

Fig 12

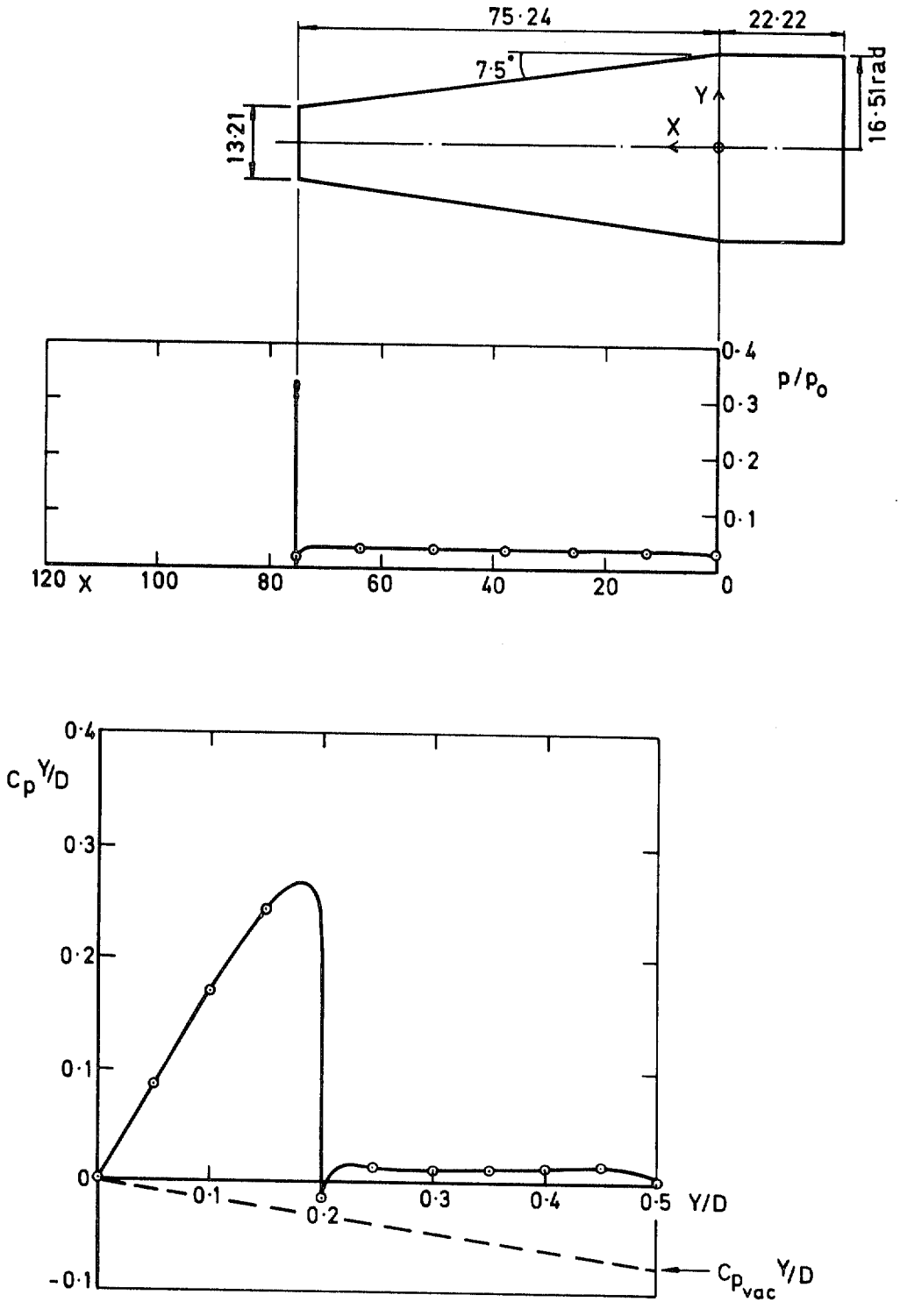

Fig 12 Experimental results. Models 22 and 23

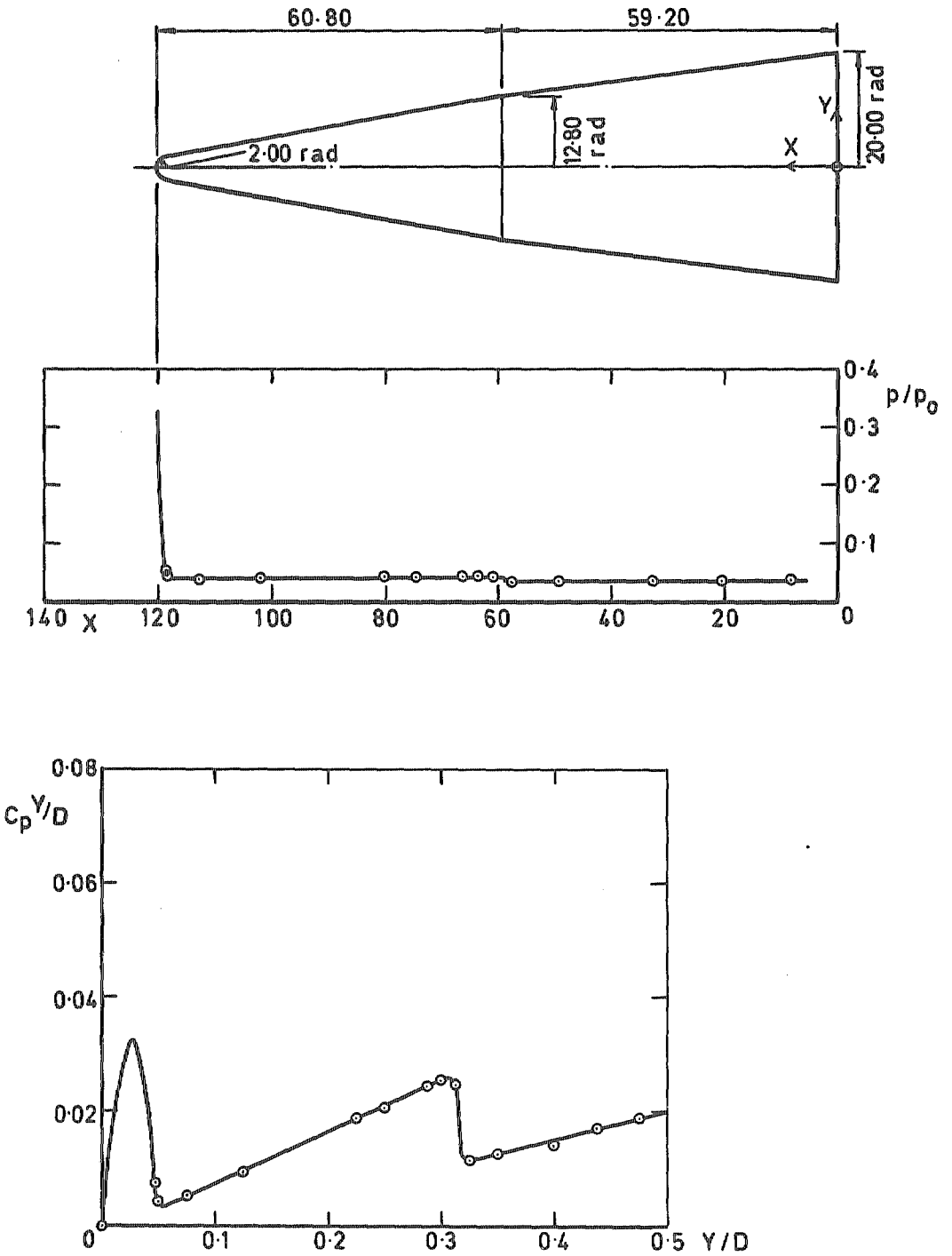

Fig 13 Experimental results. Models 24 and 25

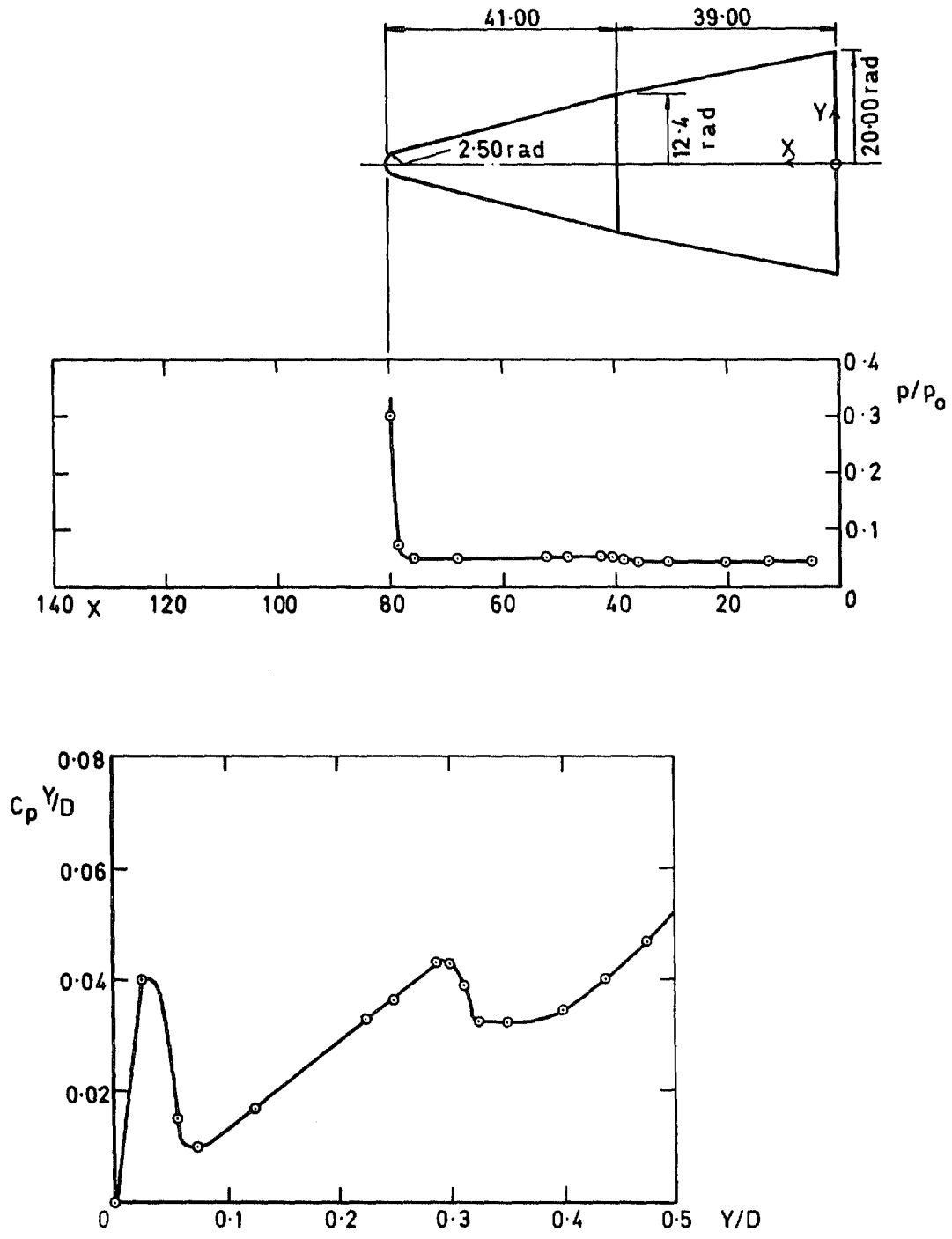

Fig 14 Experimental results. Models 26 and 27

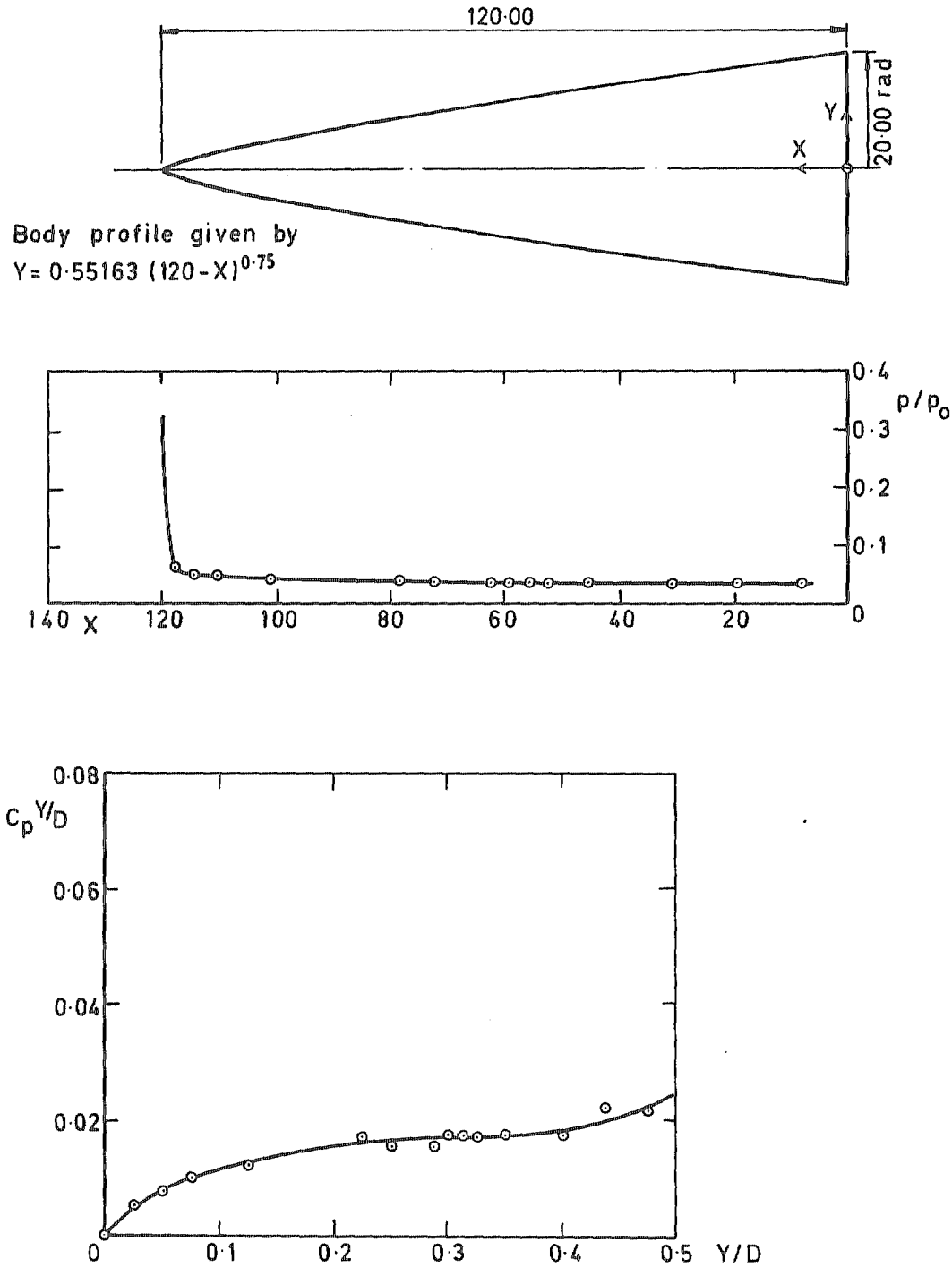

Fig 15 Experimental results. Models 28 and 29

Fig 16

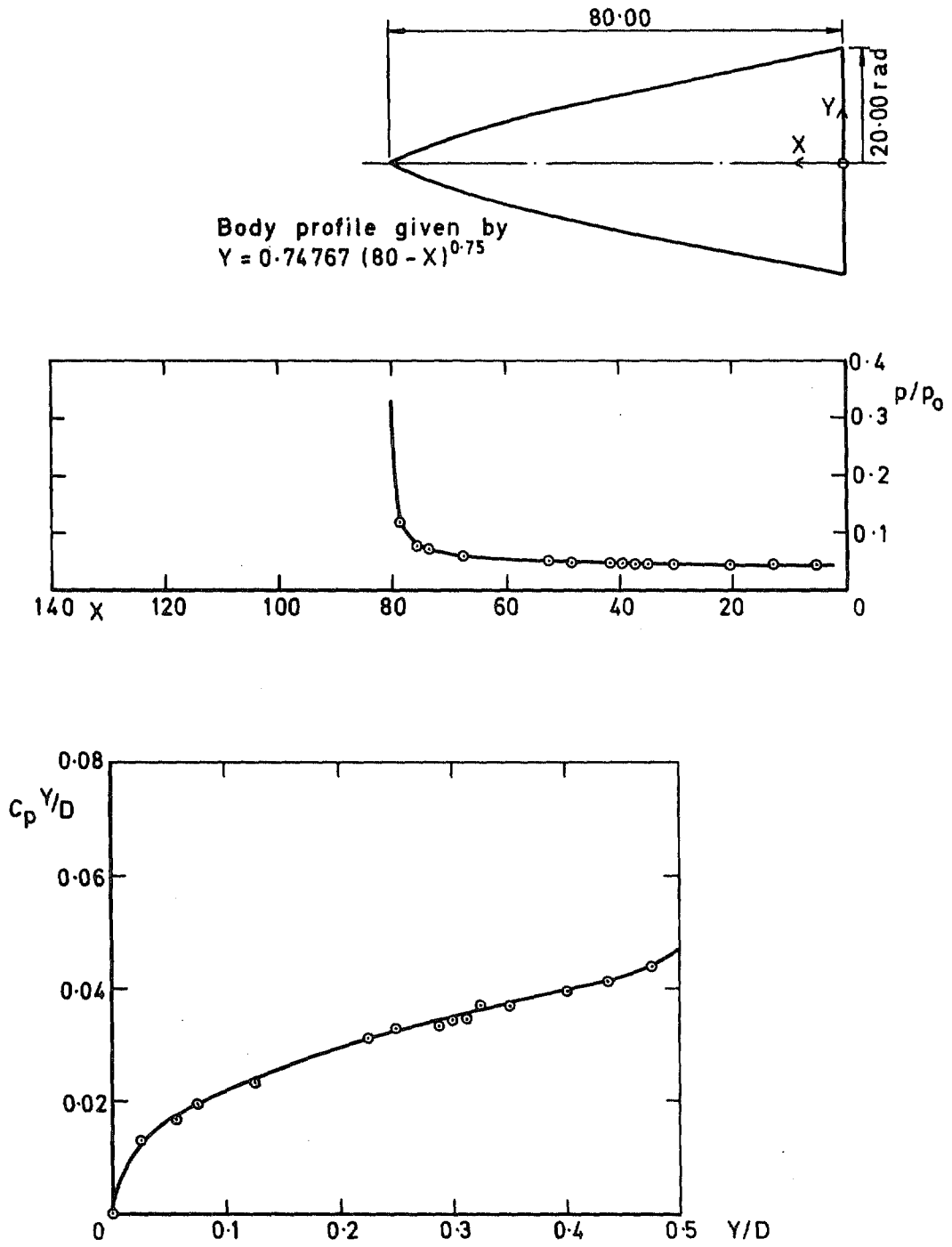

Fig 16 Experimental results. Models 30 and 31

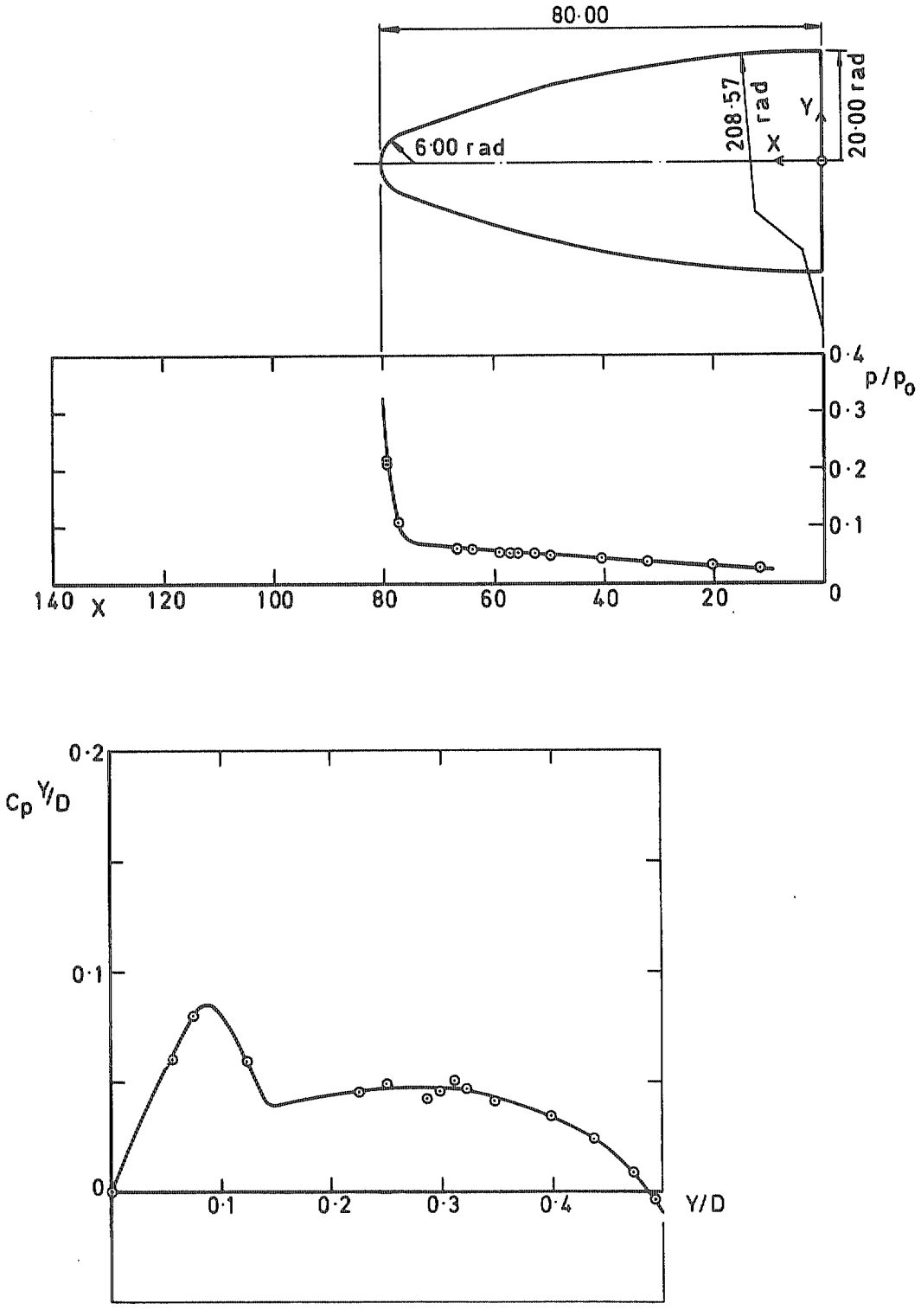

Fig 17 Experimental results. Models 32 and 33

Fig 18

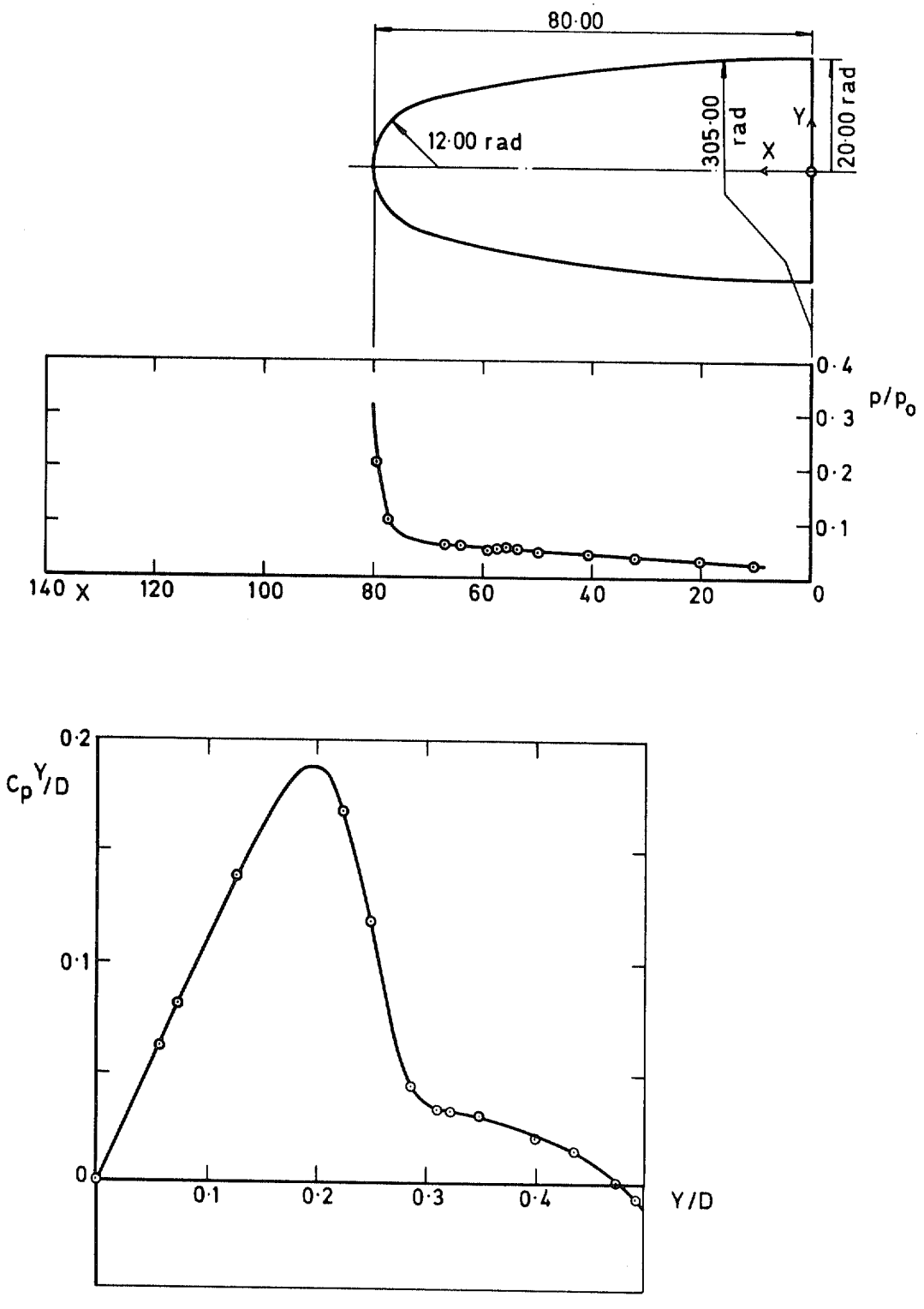

Fig 18 Experimental results. Models 34 and 35

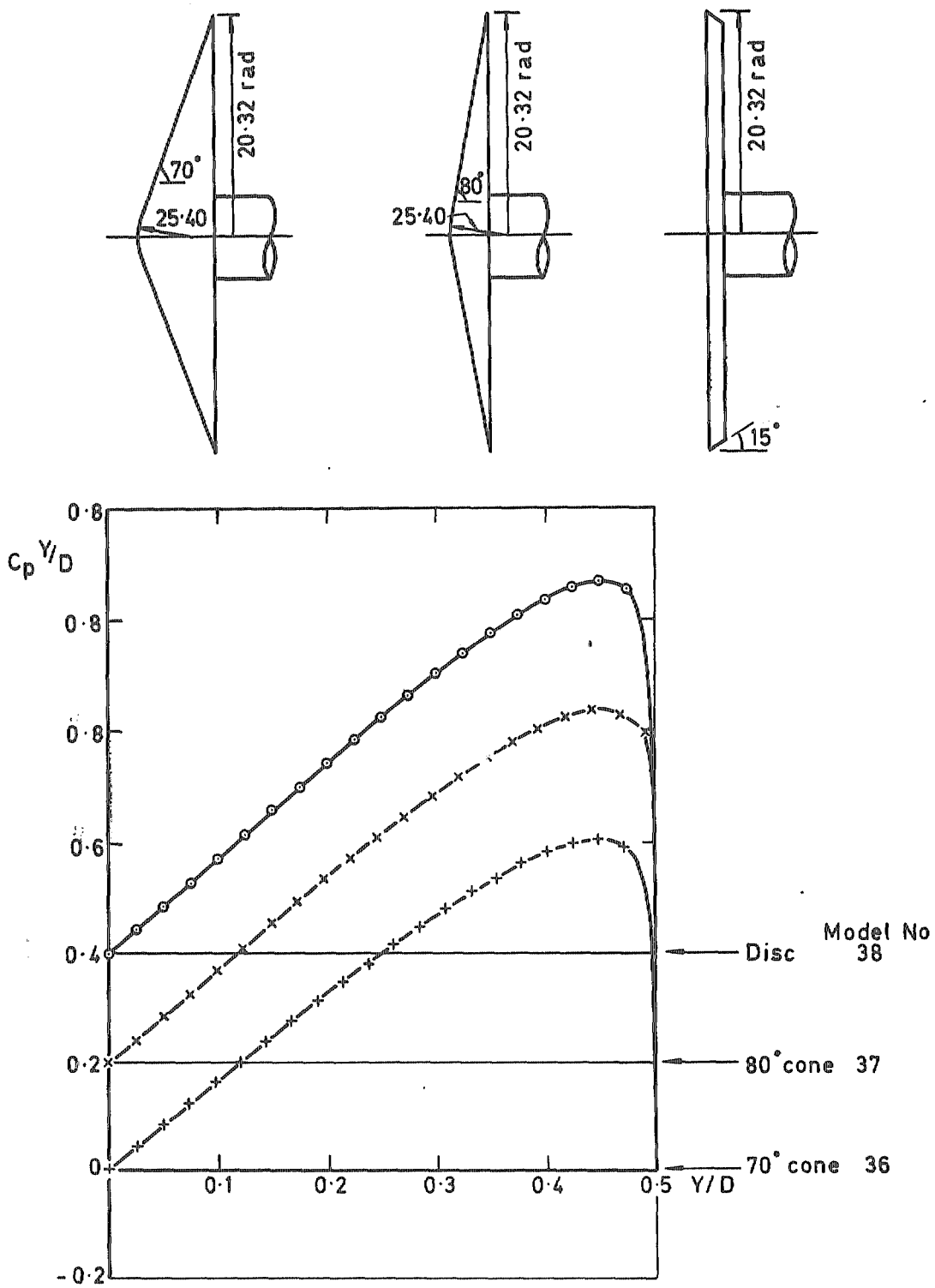

Fig 19 Experimental results from Ref 4

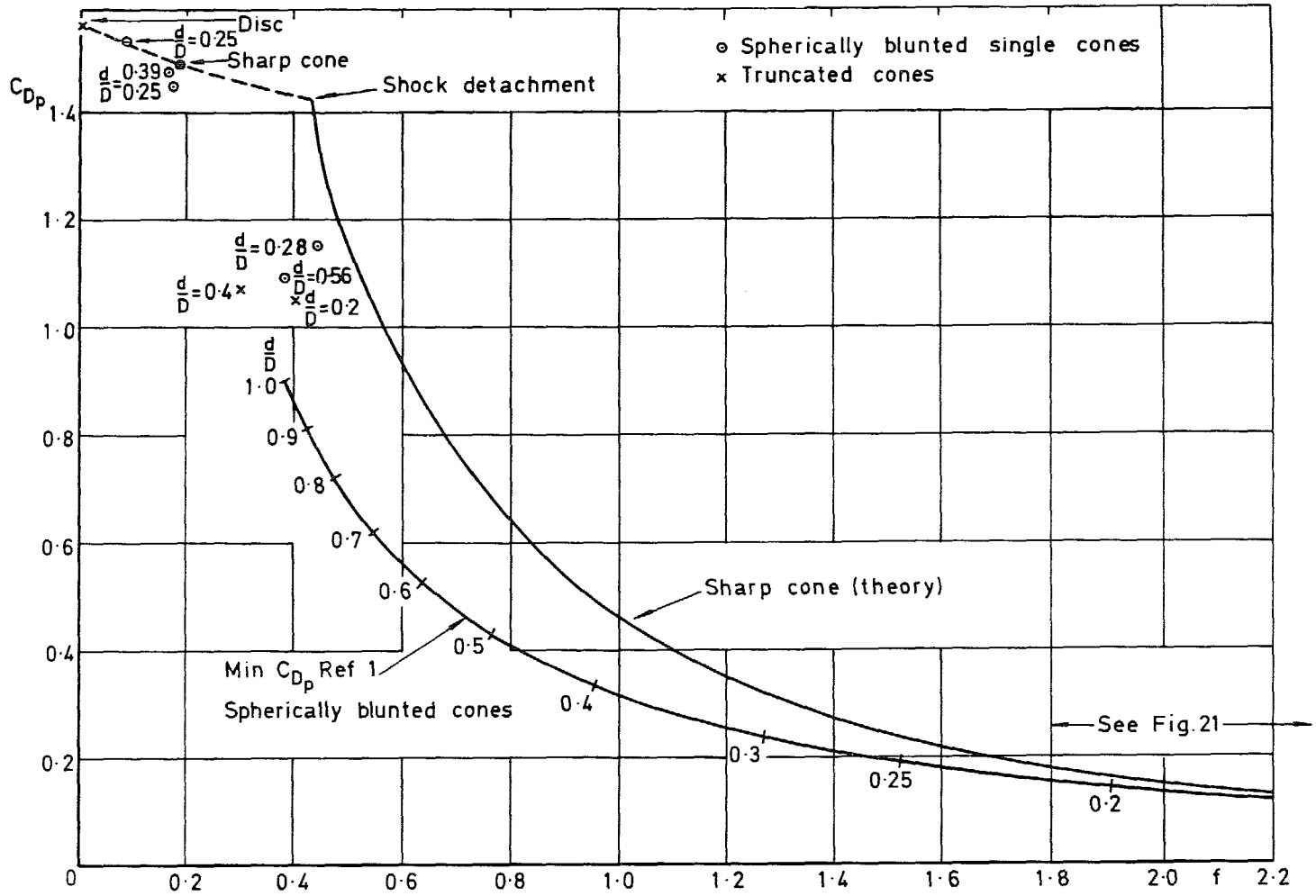

Fig 20 Comparison between integrated values of pressure drag, theoretical cone drag, and minimum obtainable drag by spherical blunting on cones from Ref 1. f = 0 to 1.8

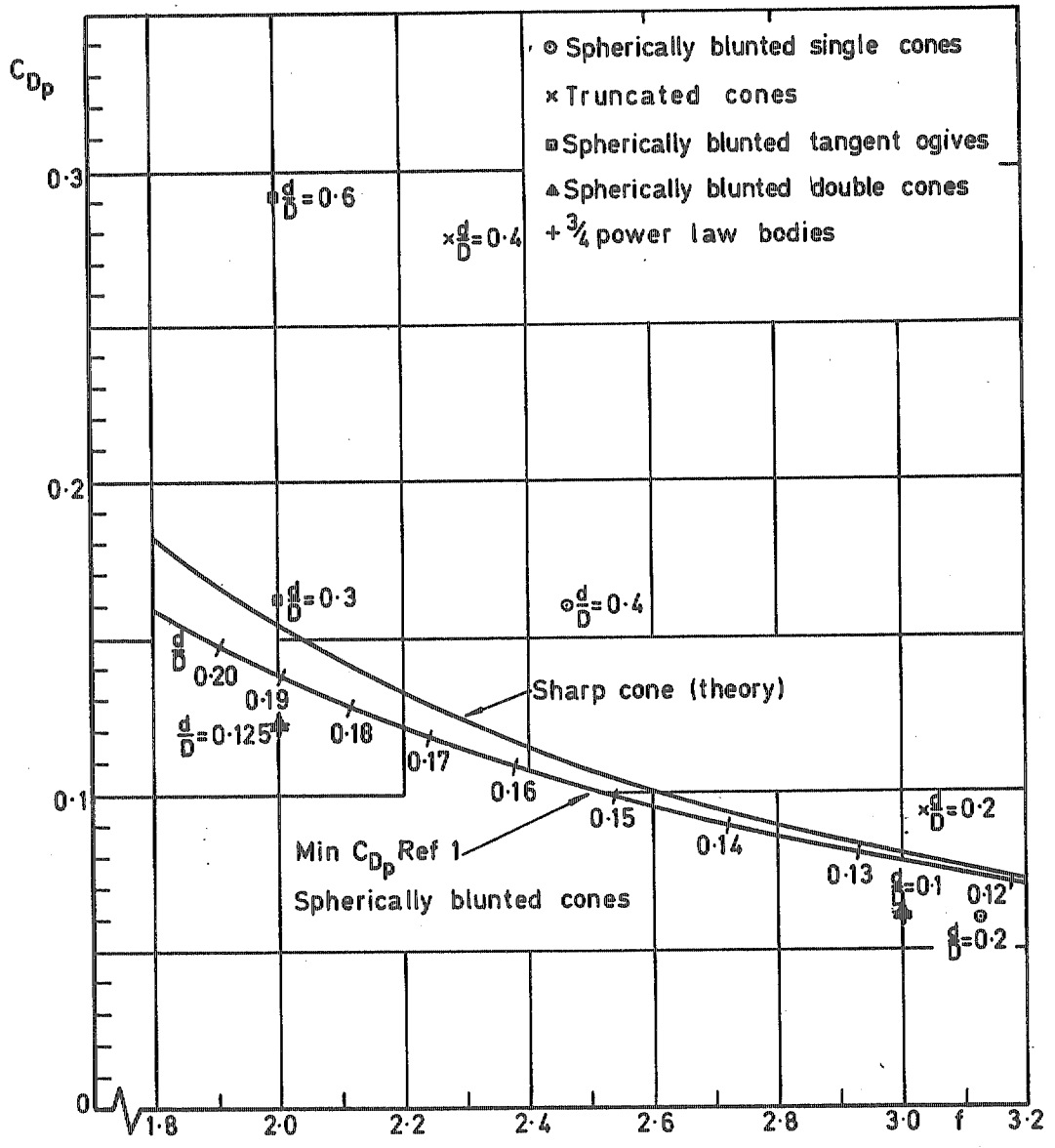

Fig 21 Comparison between integrated values of pressure drag, theoretical cone drag, and minimum obtainable drag by spherical blunting on cones from Ref 1. f = 1.8 to 3.2

Printed in England for Her Majesty's Stationery Office by the Royal Aircraft Establishment, Farnborough. Dd 596060 K4 4/80

First published 1980

HER MAJESTY'S STATIONERY OFFICE

Government Bookshops
49 High Holborn, London WC1V 6HB
13a Castle Street, Edinburgh EH2 3AR
41 The Hayes, Cardiff CF1 1JW
Brazennose Street, Manchester M60 8AS
Southey House, Wine Street, Bristol BS1 2BQ
258 Broad Street, Birmingham B1 2HE
80 Chichester Street, Belfast BT1 4JY

Government Publications are also available through booksellers

R &M No. 3849
ISBN 0114711836

R &M No. 3849

HMSO